CHEMISTRY OF MATERIALS

Article

pubs.acs.org/cm

# Role of Lone Pair Cations in Ferroelectric Tungsten Bronzes

Gerhard Henning Olsen,[†,§] Magnus Helgerud Sørby,[‡] Sverre Magnus Selbach,[†] and Tor Grande*[,†]

[†]Department of Materials Science and Engineering, NTNU Norwegian University of Science and Technology, NO-7491 Trondheim, Norway

[‡]Institute for Energy Technology, P.O. Box 40, NO-2027 Kjeller, Norway

**ABSTRACT:** The role of lone pair cations in tetragonal tungsten bronze (TTB) ferroelectrics has so far not been addressed in detail despite the importance of lone pairs for the polarization mechanism in the prototype ferroelectric perovskite $PbTiO_3$. We report a combined experimental and computational study of the effect of lone pairs in ferroelectric tungsten bronzes with particular emphasis on the important high-temperature piezoelectric lead metaniobate (PN). The ambient crystal structure of PN is revised based on X-ray and neutron powder diffraction. The most likely cation-vacancy configurations identified by the structural analysis were assessed by electron density functional theory (DFT) calculations. The ferroelectric transition was characterized by high-temperature X-ray diffraction, and the origin of the ferroelectric polarization was studied by DFT, emphasizing the relationship between polarization and cation−vacancy ordering. Covalency between Pb and O is identified as the driving force for the orthorhombic distortion of the unit cell of PN and the polarization in-plane with respect to the chains of corner-sharing octahedra. Finally, to further elucidate the role of lone pairs in ferroelectric TTBs polar lattice instabilities and resulting polarization in the TTB model system $K_4R_2Nb_{10}O_{30}$ ($R$ = La, ..., Gd, or Bi) were investigated by DFT.

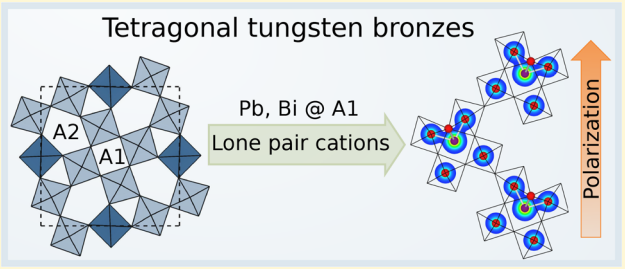


## INTRODUCTION

Oxides with tetragonal tungsten-bronze (TTB) structure constitute the second largest group of oxide ferroelectrics, surpassed only by perovskites.[1,2] They are described by the general formula $(A1)_2(A2)_4C_4(B1)_2(B2)_8O_{30}$, where the B1 and B2 cations (typically $Nb^{5+}$) and oxygen anions form a network of corner-sharing $BO_6$ octahedra.[3] The A1 and A2 sites form channels that extend throughout the crystal structure and are fully or partially occupied by cations relatively larger than the B cations such as alkali or alkaline earth metals. The C channels are narrow and can be occupied only by smaller cations such as $Li^+$ or $Nb^{5+}$ and are often completely vacant.[4,5] The TTB structure is flexible both from a chemical and structural viewpoint, resulting in a large number of compositions that crystallize in this structure. One of the simplest is lead metaniobate, $Pb_5Nb_{10}O_{30}$ (PN), which is commercially available as a high-temperature piezoelectric material, owing to its ferroelectric properties and high $T_C$ of 570 °C.[6]

Although the attractive properties of PN with TTB structure have been known for decades, the mechanism for ferroelectricity in PN has so far not been described in detail. It was recently shown that in the isostructural strontium barium niobate system, $(Sr_xBa_{1-x})_5Nb_{10}O_{30}$ (SBN), a second-order Jahn−Teller mechanism acting on $Nb^{5+}$, is responsible for the ferroelectric polarization, which is oriented along [001] in the tetragonal unit cell.[7] PN, on the other hand, has an orthorhombic unit cell with the polarization oriented along [110] with respect to the aristotype. A possible explanation for this difference is the $6s^2$ electron configuration of $Pb^{2+}$, which is known to influence the ferroelectric distortion in lead titanate, $PbTiO_3$, where Pb−O covalency leads to a tetragonal lattice strain, which in turn stabilizes the tetragonal polarization.[8] Insight into this "lone pair effect", assisted by first-principles calculations,[9] has resulted in tremendous attention toward lone pair cations such as $Bi^{3+}$ and $Sn^{2+}$ in the ongoing search for new lead-free ferroelectrics.[10] The lone pair on $Pb^{2+}$ has been suggested as the origin of the in-plane polarization in the ferroelectric TTB $Pb_2KNb_5O_{15}$ (PKN),[11] but as PKN is a filled TTB, the effect of cation−vacancy disorder still remains unclear. A further complication originates from the fact that TTBs often possess modulated crystal structures.[12,13] The existence of modulated structures, commensurate or incommensurate with the underlying crystal lattice, has been empirically linked to ferroelectricity in TTBs.[14] Incommensurate structures have been reported for certain lone-pair-containing TTBs such as $Ba_4Bi_2Ti_4Nb_6O_{30}$[15] and intermediate compositions in the solid solution system $(Pb_xBa_{1-x})_5Nb_{10}O_{30}$ (PBN),[16] but to the best of our knowledge, not for pure, undoped PN.

Here, we report on the ferroelectric mechanism in PN and on the role of lone pair cations in ferroelectric TTBs in general by combining experiments and first-principles density functional theory (DFT) calculations. The ambient temperature crystal structure of PN was first investigated by combining X-ray and neutron powder diffraction, and the influence on the

Received: May 3, 2017
Revised: July 3, 2017
Published: July 10, 2017





DOI: 10.1021/acs.chemmater.7b01817
Chem. Mater. XXXX, XXX, XXX−XXX

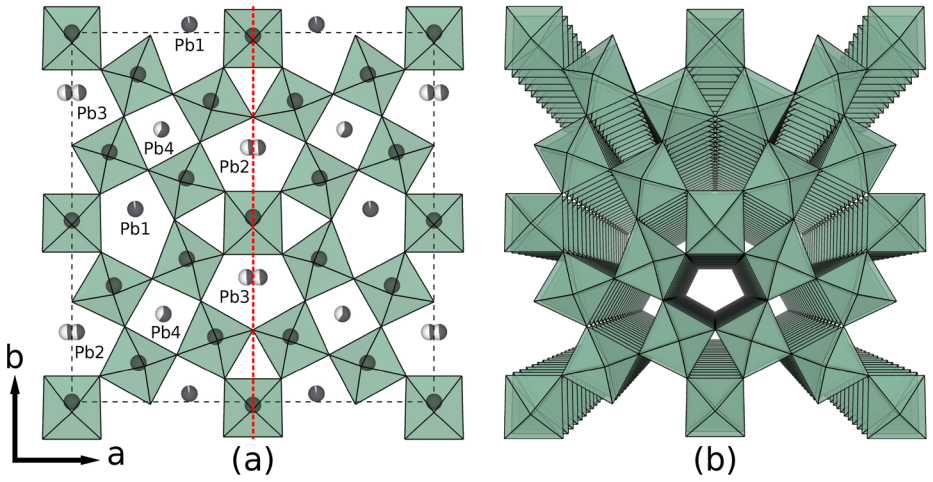


**Figure 1.** (a) Crystal structure of PN from joint refinement of X-ray and neutron powder diffraction data (space group 38, setting *Cm*2*m*). Gray spheres in channels: Pb (shading denotes occupancy), gray spheres in octahedra: Nb. The four symmetry-inequivalent Pb sites are indicated; split positions are used for the Pb2 and Pb3 sites following the model of Labbé.[32] Dashed red line marks the mirror plane normal to *a*; the 2-fold rotation axis lies in this plane at $z = \frac{1}{2}$. (b) Perspective view along a pentagonal (A2) channel, omitting Pb for clarity.

ferroelectric polarization from cation disorder and local symmetry breaking was probed by sampling the most relevant cation configurations based on the revised crystal structure. Moreover, a high-temperature X-ray study of the ferroelectric transition in PN was conducted, and we discuss how the chemical bonding in PN influences piezoelectric properties of PN-based materials. Further insight into the role of lone pairs in TTBs is gained from DFT calculations for the system $K_4R_2Nb_{10}O_{30}$ (KRN) with *R* = La, ..., Gd, or Bi, a model system which, in contrast to PN, is a fully ordered TTB system and hence free from cation−vacancy order−disorder phenomena.

## METHODS

**Powder Synthesis.** Lead metaniobate with TTB structure was made by dissolving PbO (99.999%, Sigma-Aldrich) in nitric acid and mixing in stoichiometric amounts of $Nb_2O_5$ (99.99%, Sigma-Aldrich). Two mol % of $CaTiO_3$ was added in the form of stoichiometric amounts of $CaCO_3$ (99.95%, Sigma-Aldrich) and $TiO_2$ (anatase, 99.8%, Sigma-Aldrich) to stabilize the TTB phase with respect to the rhombohedral phase as described by Sahini et al.[17] The nitric acid slurry was dried, and the powder was heated slowly to 400 °C and held at this temperature for 2 h to decompose the nitrates. The resulting oxide powder was pressed into 25 mm pellets and fired twice at 850 °C for 2 h with intermediate grinding between firings. The powder was then ball milled in ethanol for 15 h with zirconia balls, dried, pressed into 10 mm pellets, and finally fired for 1 h at 1250 °C to obtain phase-pure ferroelectric lead metaniobate, which was ground to powder.

**Diffraction Experiments and Structure Refinement.** Powder X-ray diffraction (XRD) was performed at room temperature with a Siemens D5005 diffractometer set up in Bragg−Brentano geometry with $\theta-2\theta$ scan mode. Cu $K\alpha_1$ X-rays were provided from a primary graphite monochromator, and data were collected by a Braun position sensitive detector (PSD) scanning a $2\theta$ range of 5−110° with a step size of 0.015°. Twelve 2 h scans were collected at room temperature and merged using the Bruker AXS EVA software suite.

Powder neutron diffraction data were collected at room temperature with the PUS diffractometer at the JEEP II reactor at Institute for Energy Technology in Kjeller, Norway.[18] Neutrons with a wavelength of 1.5537 Å were provided from a vertically focusing Ge monochromator, and data were collected in a $2\theta$ range of 10−130° in steps of 0.05° with two detector banks, each using 6 out of 7 horizontally stacked $^3$He-filled PSD tubes covering 20° in $2\theta$.[18]

High-temperature X-ray diffraction (HTXRD) was performed with a Bruker AXS D8 Advance set up in Bragg−Brentano geometry with $\theta-\theta$ scan mode using Cu $K\alpha$ radiation and a Våntec-1 PSD. Temperatures up to 700 °C were accessed using a high-temperature stage with a radiant heater surrounding the sample holder. A $2\theta$ range of 20−75° was scanned with a step size of 0.015°. The temperature was calibrated by recording diffractograms of $\alpha$-$Al_2O_3$ (corundum) over the same temperature range, extracting the lattice parameters by the Pawley method and fitting the parameters to polynomial expressions for the lattice parameters of corundum as a function of temperature.[19]

Rietveld refinement of the crystal structure of PN at room temperature was done with the TOPAS 5 software suite (Bruker AXS) using the X-ray and neutron diffraction data simultaneously. The background intensity was fitted to a Chebychev polynomial of minimal degree, and peak shapes were fitted to Pearson type VII or Thompson−Cox−Hastings pseudo-Voigt profiles for X-ray and neutron data, respectively. The starting point for the structure refinement was the "average" structure reported by Labbé,[20] featuring split atomic positions for Pb as an approximation to occupational disorder. Lattice parameters and atomic positions were refined according to the degrees of freedom allowed by the space group symmetry, and thermal displacement factors were refined isotropically. For the HTXRD data, a simpler Pawley fitting was used to extract the lattice parameters as a function of temperature.

**Computational Details.** Total energies were calculated by DFT as implemented in VASP[21] using the PBEsol exchange-correlation functional.[22] The projector-augmented wave (PAW) method was used[23] with PAW potentials corresponding to the electron configurations Pb ($5d^{10}6s^26p^2$), Nb ($4s^24p^64d^35s^2$), and O ($2s^22p^4$) for PN and for KRN in addition K ($3s^23p^64s^1$), Bi ($5p^65d^{10}6s^26p^3$), La−Sm ($5s^25p^65d^16s^2$), Eu−Gd ($5p^65d^16s^2$), and Tl ($5d^{10}6s^26p^1$). Wave functions were expanded in plane waves up to an energy cutoff of 550 eV, and integrals in reciprocal space were sampled on a 2 × 2 × 6 Monkhorst−Pack grid[24] for the 45-atom unit cell (in the case of PN) and reduced accordingly for supercells. Structures were relaxed until the Hellmann−Feynman forces on the ions converged to below $10^{-4}$ eV $Å^{-1}$.

Configurational aspects of the inherently disordered unfilled TTB structure were handled in a manner similar to what was done for PN as well as for the analogous lead-free TTB niobates $Sr_5Nb_{10}O_{30}$ (SN) and $Ba_5Nb_{10}O_{30}$ (BN) in our previous work.[7,25] In the previous work, configurational analysis was based on a 90-atom, 1 × 1 × 2 supercell of the 45-atom aristotype unit cell. Here, the starting point is the 90-atom unit cell for PN with average space group symmetry *Cm*2*m*, which was also used for the structural refinements. Configurations in this cell are sampled based on refined cation occupancies, and the relevant configurations are used for computational studies. For the KRN


DOI: 10.1021/acs.chemmater.7b01817
Chem. Mater. XXXX, XXX, XXX−XXX

system, structural data for the unfilled $(Sr,Ba)_5Nb_{10}O_{30}$ system[26] was used as the starting point, in lieu of experimental data on the KRN system itself. This is a reasonable approximation, as the TTB framework is rigid and thus not very sensitive to small, local distortions and hence not likely to get trapped in a local energy minimum because of a poor starting point. A paraelectric aristotype structure was found by searching for a pseudosymmetric structure with space group *P*4/*mbm*,[27] and lattice parameters and atomic positions were subsequently optimized under the constraints imposed by the space group symmetry.

Gamma-point phonons were calculated by the direct method as implemented in PHONOPY[28] using atomic displacements of 0.01 Å for calculation of interatomic forces. Starting from high-symmetry structures with the aristotype space group symmetry *P*4/*mbm*, dynamically unstable modes were manifested as phonons with imaginary frequencies. Polar structures were obtained by displacing atoms at fixed volume according to the eigenvectors of the unstable modes and then relaxing the atomic positions and lattice parameters starting from a point close to the energy minimum.[29] For doubly degenerate modes, linear combinations were taken corresponding to the high-symmetry directions in order parameter space.[30]

## RESULTS

**Refinement of PN at Ambient Temperature.** The room-temperature crystal structure of ferroelectric lead metaniobate is shown in Figure 1a based on simultaneous refinement of X-ray and neutron diffraction data (goodness of fit: $R_p$ = 8.29%, $R_{wp}$ = 10.70%, $\chi^2$ = 1.46). The two diffractograms and the refined profiles are shown in Figure 2, and the atomic positions and site

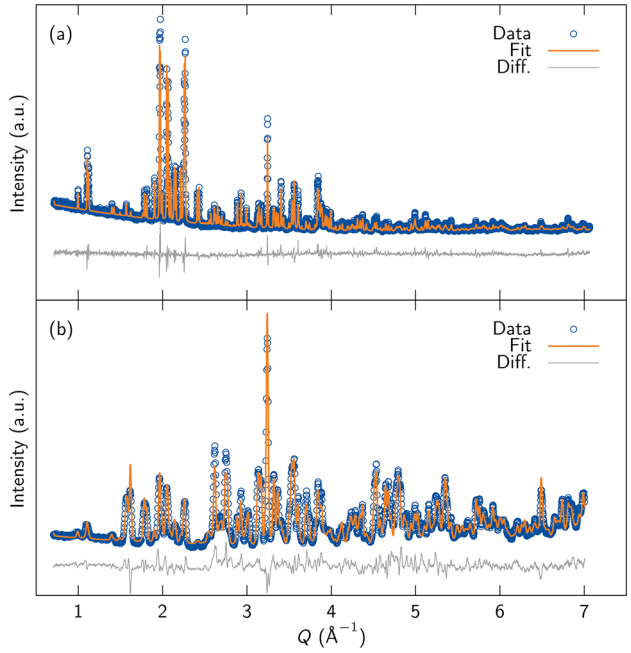


**Figure 2.** (a) Powder X-ray and (b) powder neutron diffractograms for PN at ambient temperature plotted as a function of the scattering vector ($Q = 2\pi/d$). Refinement profiles and difference curves are shown for simultaneous refinement of both data sets.

occupancies determined by the refinement are presented in Table 1. The neutron diffraction data revealed that the crystal structure of PN is not as distorted as previously reported[20,31] with less deformed $NbO_6$ octahedra and a more regular shape of the channels along the "pseudo-tetragonal" *c*-axis. A view along this axis is displayed in Figure 1b, demonstrating the anisotropy of the structure. The split-atom model for PN used here was first introduced by Labbé[20,32] as an approximation to the apparent occupational disorder on the A2 sites in this structure. In this model, all Pb atoms are in 4e Wyckoff positions but with occupancies constrained so that the total number of Pb atoms sums to 10 for the 90-atom *Cm*2*m* cell. In our refinement, we additionally constrain the Pb occupancy to be the same for all the A2 sites, effectively refining the distribution of Pb between A1 and A2 sites. In the original work, the occupancy of Pb was not refined, it was simply assumed that Pb preferentially occupies the pentagonal (A2) sites, leading to an occupation of $\frac{1}{2}$ for the square (A1) sites. The refined occupancies (Table 1) confirm that this assumption holds up within the framework of this crystallographic model.

**Spontaneous Polarization in PN.** As a first approach, the spontaneous polarization was calculated based on a simple point-charge model where the polarization is given by[33]

$$\mathbf{P}_s = P_y = \frac{e}{V}\sum_i \gamma_i Z_i \Delta y_i \quad (1)$$

where $e$ and $V$ are, respectively, the elementary charge and the volume of the unit cell, and the sum is taken over all atomic sites in the cell taking multiplicities into account. $\gamma_i$ is the fractional occupancy of each site (occ. in Table 1); $Z_i$ is the nominal ionic charge assuming $Pb^{2+}$, $Nb^{5+}$ and $O^{2-}$, and $\Delta y_i$ is the atomic displacement along $y$ relative to a nonpolar reference structure (the polarization is confined to the $y$ direction by symmetry). To find a suitable reference structure, we construct a minimal nonpolar supergroup of the experimental *Cm*2*m* structure, which in this case has space group symmetry *Cmmm*.[27] This simple model gives a spontaneous polarization of 40 $\mu$C cm$^{-2}$ for the experimentally determined structure.

A corresponding DFT calculation of the spontaneous polarization cannot be performed without making approximations to the crystallographic data. More specifically, cation configurations must be chosen such that the occupancy of each atom is either zero or one. An occupancy of Pb of 0.96 at the A2 sites and 0.59 at the A1 sites was determined by the structural refinement (Table 1). The cation configurations that are most relevant for further consideration are therefore the ones where all of the A2 sites and half of the A1 sites are occupied by Pb. There are four configurations of this type for the 90-atom *Cm*2*m* cell; these configurations are presented in Table 2 where they are numbered 1−4, and the local space group symmetry is given for each case.[34] In this context, local space group symmetry refers to the lowering of symmetry from the average *Cm*2*m* structure when the Pb atoms are localized as described above. For the configurations considered here, the space group symmetry is lowered to orthorhombic $Pb2_1m$ or *Pm*2*m* or monoclinic *Pm* (Table 2). The symmetry affects the properties in the sense that the monoclinic structure allows for a spontaneous polarization along any in-plane direction, whereas the orthorhombic structures have a unique polar direction, *b* in the setting used here, along a twofold rotation or screw axis.

The atomic positions were optimized for the four relevant cation configurations described above with the split atomic positions replaced by single Pb atoms in the average positions (in the mirror plane). The optimization of atomic positions was performed under the symmetry constraints imposed by the local space group symmetry dictated by the cation config-


DOI: 10.1021/acs.chemmater.7b01817
Chem. Mater. XXXX, XXX, XXX−XXX

**Table 1. Atomic Positions for PN Based on Joint Refinement of X-ray and Neutron Diffraction Data Given in the *Cm2m* Setting of Space Group 38 (90 atoms; 2 units of $Pb_5Nb_{10}O_{30}$)[a]**

| atom | WP | $x$ | $y$ | $z$ | occ. | $B_{iso}$ |
|---|---|---|---|---|---|---|
| Pb1 (A2) | 4e | 0.3246(2) | 0.0222(5) | $\frac{1}{2}$ | 0.955(3) | 0.44(6) |
| Pb2 (A2) | | 0.0135(5) | 0.1889(5) | $\frac{1}{2}$ | $\frac{1}{2} \times 0.955(3)$ | |
| Pb3 (A2) | | 0.4818(4) | 0.3373(5) | $\frac{1}{2}$ | $\frac{1}{2} \times 0.955(3)$ | |
| Pb4 (A1) | | 0.2529(6) | 0.2377(7) | $\frac{1}{2}$ | 0.590(7) | 1.6(2) |
| Nb1 | 2a | 0 | 0 | 0 | 1 | 0.42(3) |
| Nb2 | | 0 | 0.4913(7) | 0 | 1 | |
| Nb3 | 4d | 0.1840(4) | 0.1055(6) | 0 | 1 | |
| Nb4 | | 0.3172(4) | 0.3869(5) | 0 | 1 | |
| Nb5 | | 0.3961(4) | 0.1762(6) | 0 | 1 | |
| Nb6 | | 0.1162(4) | 0.3150(6) | 0 | 1 | |
| O1 | 2b | 0 | 0.9714(7) | $\frac{1}{2}$ | 1 | 1.17(3) |
| O2 | | 0 | 0.4794(10) | $\frac{1}{2}$ | 1 | |
| O3 | 4e | 0.2009(5) | 0.0966(7) | $\frac{1}{2}$ | 1 | |
| O4 | | 0.3323(5) | 0.3774(6) | $\frac{1}{2}$ | 1 | |
| O5 | | 0.4019(5) | 0.1657(7) | $\frac{1}{2}$ | 1 | |
| O6 | | 0.1146(5) | 0.2902(7) | $\frac{1}{2}$ | 1 | |
| O7 | 4d | 0.0768(5) | 0.0698(7) | 0 | 1 | |
| O8 | | 0.1460(5) | 0.2034(7) | 0 | 1 | |
| O9 | | 0.2170(4) | 0.9932(7) | 0 | 1 | |
| O10 | | 0.2897(5) | 0.1275(7) | 0 | 1 | |
| O11 | | 0.4222(5) | 0.0622(7) | 0 | 1 | |
| O12 | | 0.0811(6) | 0.4054(7) | 0 | 1 | |
| O13 | | 0.2214(5) | 0.3331(6) | 0 | 1 | |
| O14 | | 0.3561(5) | 0.2731(7) | 0 | 1 | |
| O15 | | 0.4191(5) | 0.3991(7) | 0 | 1 | |
| O16 | 2a | 0 | 0.6943(9) | 0 | 1 | |
| O17 | | 0 | 0.2708(8) | 0 | 1 | |

[a]A1 and A2 refer to square and pentagonal sites in the TTB structure. WP, Wyckoff position; occ., occupancy; $B_{iso}$, isotropic thermal displacement factors (constrained to be the same for all Nb, all O, and all Pb on A2 sites). Occupancies are refined for Pb and constrained to be the same for the A2 sites (Pb2 and Pb3 are split sites, hence the occupancy of these sites is half of the occupancy of the Pb1 site). Lattice parameters: $a$ = 17.6483(5) Å, $b$ = 17.9487(5) Å, $c$ = 3.87109(10) Å.

**Table 2. Cation Configurations Possible for the $\sqrt{2} \times \sqrt{2} \times 1$ Supercell Considered for PN[a]**

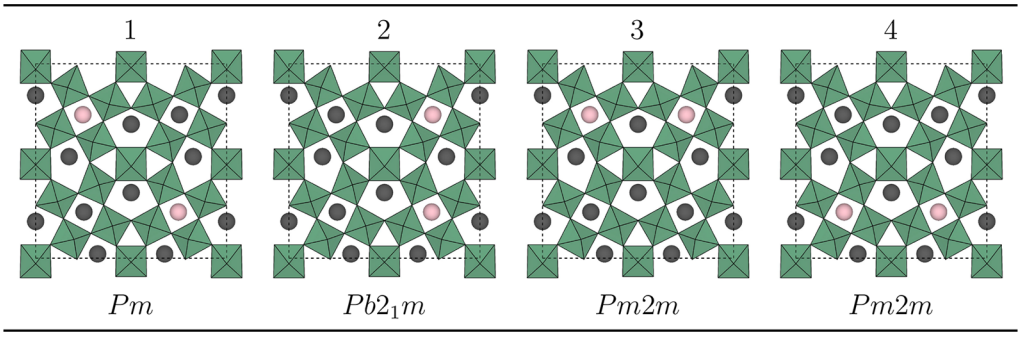


[a]Light colored spheres: vacancies. Local space group symmetry of each polar configuration is given (average symmetry *Cm2m*). Setting and orientation of the cell is the same as that in Figure 1.

urations, while the lattice parameters were kept fixed at the experimental values (Table 1). The resulting energy landscape is presented in Figure 3a, which shows that configurations 1 and 2 possess an energy per 90-atom cell about 0.5 eV lower than that of configurations 3 and 4. It should also be noted that configuration 1, while having the lowest symmetry (monoclinic *Pm*) and hence the highest number of atomic degrees of freedom, is not the lowest-energy configuration. The energy difference between configurations 1 and 2, however, is on the order of 7 meV per Pb atom, which is small enough that these configurations should be regarded as equally energetically favorable. The same holds for a comparison of the configurations 3 and 4. At the same time, the energy difference between the high- and low-energy configurations corresponds


DOI: 10.1021/acs.chemmater.7b01817
Chem. Mater. XXXX, XXX, XXX−XXX

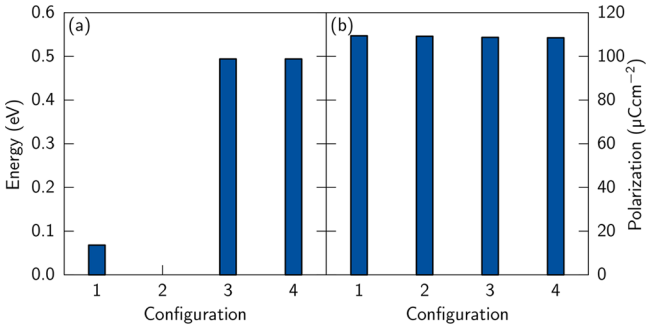


**Figure 3.** (a) Energy landscape for the four cation configurations considered for PN (Table 2) after optimizing atomic positions at constant experimental lattice parameters. Energies given per 90-atom supercell relative to configuration 2 which has the lowest energy. (b) Spontaneous polarization for the for cation configurations.

to 43−49 meV per Pb atom, suggesting that order−disorder between all four configurations is possible at temperatures relevant for synthesis of PN.

The crystal structure of PN allows for an in-plane spontaneous polarization, and the calculated polarization of the four relevant cation configurations is presented in Figure 3b. The polarization is high, about 109 $\mu$C cm$^{-2}$ for all the four configurations (ranging from 108.5 to 109.4 $\mu$C cm$^{-2}$). Configurations 2−4, which are locally orthorhombic, have a spontaneous polarization that lies strictly along the 2-fold rotation or screw axis (along $b$ in the $Cm2m$ cell). Configuration 1, which is monoclinic, has the main component of the polarization in the same direction in addition to a small component along $a$, which leads to the net polarization forming a 1.5° angle with $b$ for this configuration.

The mechanism stabilizing the in-plane polarization can be understood from the charge density, shown for configuration 2 in Figure 4, which provides an intuitive interpretation of the chemical bonding in the material. Covalent bonding has a significant influence on the structural distortion, and Pb bonds more strongly to four of the surrounding oxygen anions (Figure 4a). This leads to a substantial displacement of Pb inside both

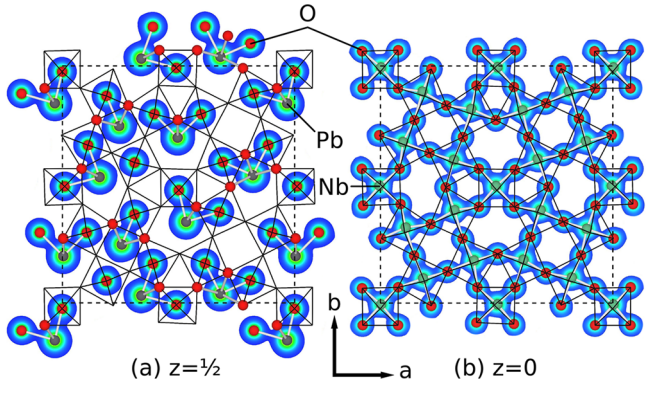


**Figure 4.** Charge density sections for PN optimized in configuration 2. (a) $z = \frac{1}{2}$ plane, showing the Pb−O bonds stabilizing displacement of Pb in the A1 and A2 channels. Note that oxygens above and below the $z = \frac{1}{2}$ plane are shown as atoms *not* surrounded by a charge density. (b) $z = 0$ plane, showing the Nb−O bonds that define the $NbO_6$ octahedra (outline of octahedra drawn with black lines in both panels). The charge density isosurfaces are drawn at 2 and 6% of the maximum charge density, respectively.

the square (A1) and the pentagonal (A2) channels, while the displacement of Nb inside the $NbO_6$ octahedra (Figure 4b) is less pronounced.

**Lattice Parameters of PN Across the Ferroelectric Phase Transition.** The high-temperature behavior of PN was investigated by HTXRD, and representative diffractograms are displayed in Figure 5. As the temperature is lowered below the

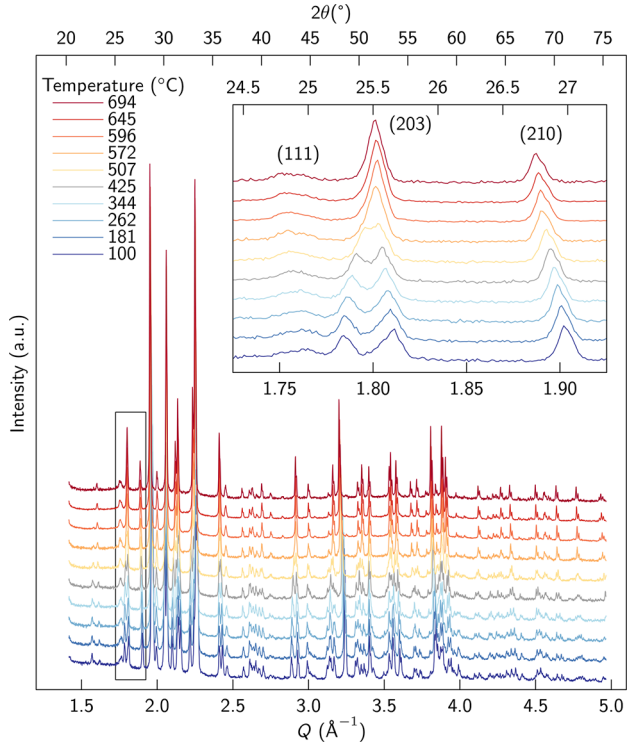


**Figure 5.** Diffractograms of PN at different temperatures. $2\theta$ scale for Cu K$\alpha$ radiation given on top axis. Inset: magnification of the data set marked with a rectangle in the main plot.

phase transition, some of the diffraction lines are split as a consequence of the transition from tetragonal to orthorhombic symmetry. The ferroelectric transition occurs at $T_C = (595 \pm 5)$ °C, compared to literature values from 534 to 570 °C.[6,17,35] The lattice parameters of PN were obtained by Pawley fitting with space group symmetry $P4/mbm$ above $T_C$ and $Cm2m$ below, as shown for two selected diffractograms in Figure 6. The lattice parameters are presented as a function of temperature in Figure 7a. In the tetragonal paraelectric phase, the two in-plane lattice parameters are identical ($a = b$) but become different ($b > a$) below $T_C$, when the symmetry is reduced to orthorhombic $Cm2m$. Extrapolation of the in-plane lattice parameter of the paraelectric phase (Figure 7a) coincides perfectly with the $a$ lattice parameter of the ferroelectric phase, and it is therefore logical to define a spontaneous strain[36] for the $Cm2m$ phase as $e_{22} = (b - a)/a$, as shown in Figure 7b. The notation $e_{22}$ reflects that it is a strain along $b$, the polar direction, in the ferroelectric $Cm2m$ phase, but it can equivalently be described as a shear strain along [110] referred to the aristotype $P4/mbm$ structure. The strain has a magnitude of 1.7% at room temperature. For comparison, the ambient-temperature spontaneous strain in PKN is around 1.2%,[11] while the prototypical perovskites $KNbO_3$, $BaTiO_3$, and $PbTiO_3$ have strains of 0.5, 1, and 6%, respectively.[37,38]



DOI: 10.1021/acs.chemmater.7b01817
Chem. Mater. XXXX, XXX, XXX−XXX

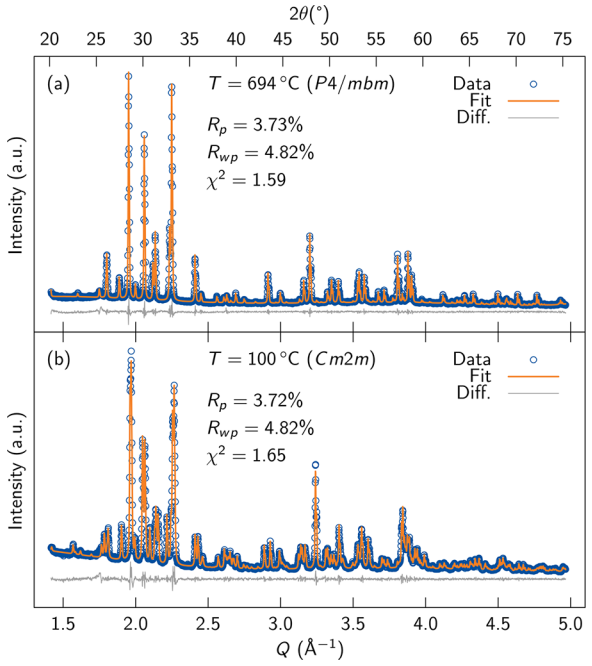


**Figure 6.** Pawley fitting of X-ray diffractograms recorded above (a) and below (b) the ferroelectric transition for PN. $2\theta$ scale for Cu K$\alpha$ radiation given on the top axis.

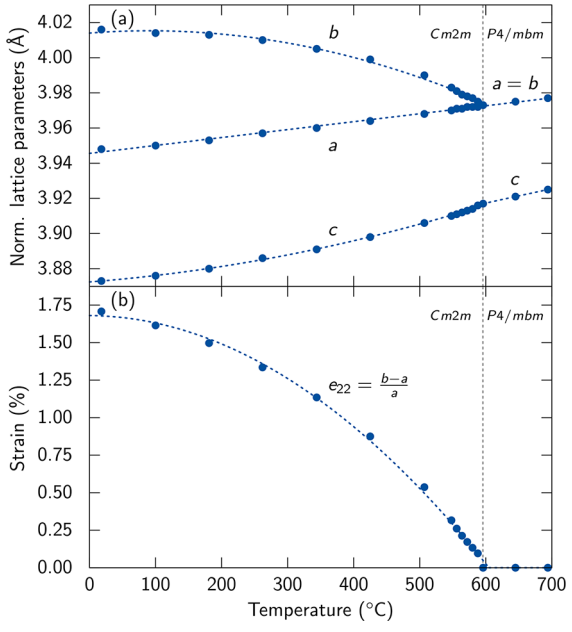


**Figure 7.** (a) Temperature evolution of the lattice parameters for PN. $a$ and $b$ are scaled by a factor $1/(2\sqrt{10})$ ($T < T_C$) or $1/\sqrt{10}$ ($T > T_C$) so that all dimensions are directly related to the size of an $NbO_6$ octahedron. (b) Spontaneous strain as a function of temperature.

**Effect of Lone Pair Cations in the KRN System.** To further elucidate the role of lone pairs in TTBs, calculations were performed for the model system KRN ($K_4R_2Nb_{10}O_{30}$ with $R$ = La, ..., Gd, or Bi). The KRN compounds are filled, ordered TTBs,[39] which eliminates the need to consider cation−vacancy disorder, while at the same time making it possible to compare the effects of cation size and the presence of lone pair cations. The structures were first optimized by relaxing the atomic positions and lattice parameters within the symmetry constraints of the aristotype space group $P4/mbm$. The resulting lattice parameters and cell volumes are displayed in Figure 8a and can generally be seen to increase with increasing

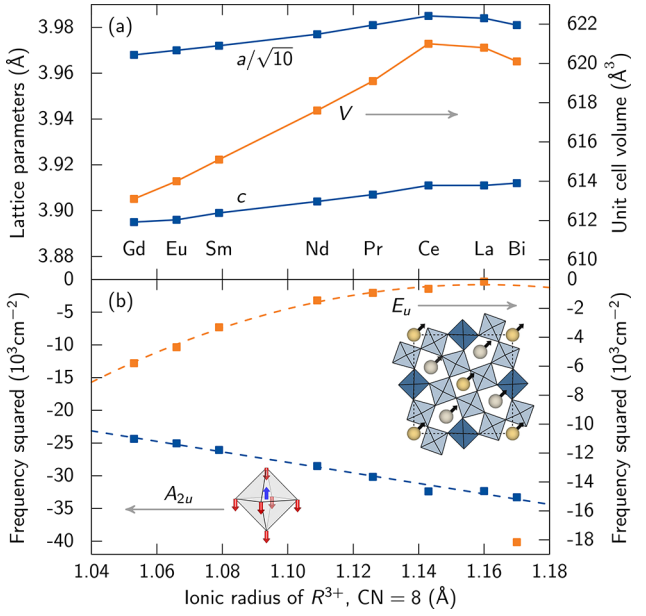


**Figure 8.** (a) Lattice parameters and volume for the KRN series in the aristotype space group $P4/mbm$. The in-plane lattice parameter is reported as $a/\sqrt{10}$ to make it directly comparable to the $c$ parameter (both related to the size of an $NbO_6$ octahedron). (b) Squared frequencies for unstable polar phonons in KRN. Two unstable phonons exist for all compounds, one giving rise to a polarization along $z$ ($A_{2u}$, left axis) and the other in the $xy$ plane ($E_u$, right). The displacement patterns of the two modes are drawn schematically. Note the deviation from the trend for the $E_u$ mode in KBiN.

radius of $R$. The only exception to this trend is a slight volume contraction for the Bi compound, mainly due to a contraction of the in-plane lattice parameter.

Phonon calculations for the optimized high-symmetry KRN structures revealed two kinds of unstable modes, both polar, transforming like the irreducible representations (irreps) $A_{2u}$ and $E_u$. The $A_{2u}$ mode, which takes the structure to the isotropy subgroup $P4bm$, consists mainly of Nb displacements within the $NbO_6$ octahedra, leading to a polarization along $z$. This type of instability was also found to exist for all possible cation configurations in the unfilled TTB ferroelectric SBN.[7] The doubly degenerate $E_u$ mode mainly involves in-plane displacements of the A1 and A2 cations inside the channels, giving a polarization in the $xy$ plane. There are three symmetry-inequivalent order parameter directions for this mode: ($a$,0), ($a$,$a$), and ($a$,$b$), corresponding to the isotropy subgroups $Pb2_1m$, $Cm2m$, and $Pm$, respectively, where the $Pb2_1m$ solution was found to have the lowest energy. The frequencies of these modes are plotted as a function of the $R^{3+}$ radius in Figure 8b, which also shows schematic illustrations of the displacement patterns described above. The frequency of the out-of-plane polar ($A_{2u}$) mode follows a linear trend, while the in-plane ($E_u$) mode shows a parabolic dependency on the cation radius. The two modes display different trends in the sense that the $A_{2u}$ mode is most strongly unstable (largest imaginary frequency) for the largest $R^{3+}$ cations (La and Bi), while the $E_u$ mode is most strongly unstable for the smallest cation (Gd). The exception is the $E_u$ instability for the Bi compound, abbreviated


DOI: 10.1021/acs.chemmater.7b01817
Chem. Mater. XXXX, XXX, XXX−XXX

KBiN in the following, which has the most strongly imaginary frequency of all the cases investigated.

Displacement of atoms along the unstable mode eigenvectors leads to a lowering of the energy in all cases, as demonstrated in Figure 9. Consistent with the imaginary frequencies of the

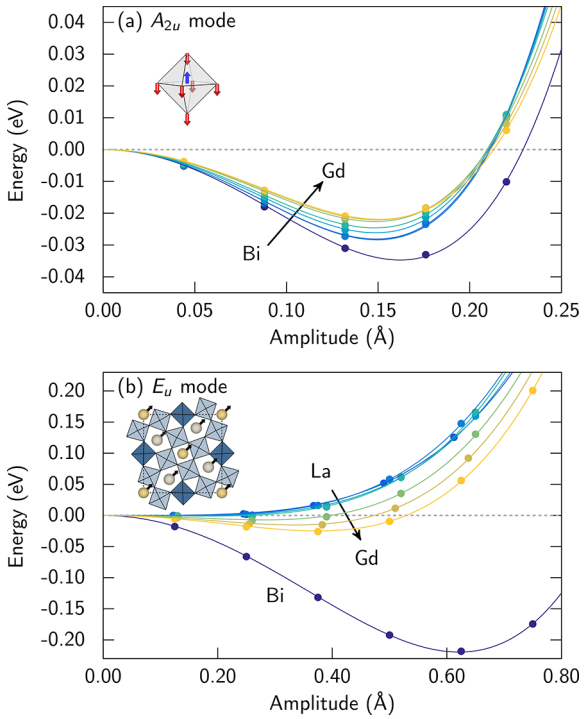


**Figure 9.** Energy as a function of mode amplitude[40] for the $A_{2u}$ (a) and $E_u$ (b) phonons in KRN. Note the different energy scales. Arrows indicate decreasing ionic radius.

modes (Figure 8b), the Bi compound experiences the largest energy lowering for the $A_{2u}$ mode (Figure 9a), and the Gd compound the least. For the $E_u$ mode (Figure 9b), the trend for the phonon frequencies is also mirrored by the energies, with KBiN deviating substantially from the other compounds by being the only compound with a significant energy lowering of 0.22 eV per unit cell. Starting from a point close to the minimum on the energy surface for the $E_u$ mode in KBiN (at around 0.62 Å in Figure 9b), relaxation of the lattice parameters and atomic positions leads to a polar structure with space ground symmetry $Pb2_1m$ and an in-plane polarization of 68 $\mu$C cm$^{-2}$ along $b$. This is a high value, around two-thirds of that calculated for PN (Figure 3b). As for PN, calculation of the polarization in KBiN according to a simple point-charge model, eq 1, gives a lower value of 33 $\mu$C cm$^{-2}$. The charge density of relaxed KBiN, displayed in Figure 10, demonstrates that the chemical bonding is similar to that in PN (Figure 4) with covalent Bi–O bonds contributing to stabilization of the in-plane polarization in addition to displacement of $Nb^{5+}$ within the $NbO_6$ octahedra. $K^+$ is, however, not ferroelectrically active and is more or less centrosymmetrically positioned in the A2 channels also in the polar KBiN structure.

## DISCUSSION

**Crystal Structure of PN.** The combination of X-ray and neutron diffraction data improved the quality of the description of the crystal structure of PN relative to that from previous data (Table 1). Compared to structure data based solely on X-ray

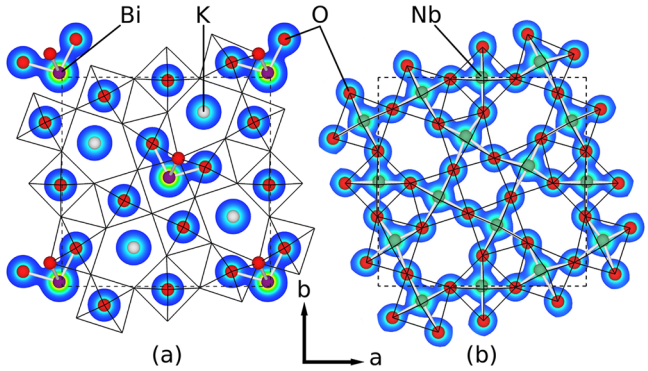


**Figure 10.** Charge density sections for KBiN in the polar space group $Pb2_1m$ (polarization along $b$); compare to Figure 4. (a) Bi–O plane and (b) Nb–O plane; both panels show the outline of the $NbO_6$ octahedra (black lines). Isosurface values are 2 and 4% of maximum charge density, respectively.

diffraction, the present work provides a good description also of the oxygen positions, which in practice leads to more physically realistic atomic arrangements with $NbO_6$ octahedra less deformed than those in previous reports on PN.[20,31] Similar results have recently been reported for the stable rhombohedral polymorph of PN.[41] The temperature factors, $B_{iso}$ in Table 1, are relatively large for Pb4 and O at 1.6 ± 0.2 and 1.17 ± 0.03, respectively. Pb4 is located on the A1 site in the TTB structure, and its average occupancy of 0.59 creates the possibility for local disorder, which is here accounted for by probing the most relevant cation configurations as described above. The oxygen positions are also affected by the disordered cation configurations, which is reflected in higher temperature factors also for oxygen. It can be noted that in the original investigation of strontium barium niobate (SBN) by Jamieson,[3] it was deemed necessary to introduce split atomic positions for the oxygens above and below Nb along the tetragonal axis to get a reasonable fit for the oxygen thermal factors. In the case of SBN, this oxygen disorder was later shown to be related to incommensurately modulated structures.[12] As mentioned in the introduction, modulated structures are a common feature among ferroelectric TTBs,[14−16] and while it has not been reported for pure ferroelectric PN to the best of our knowledge, the possibility cannot be excluded.

The structure refinement used in this work relies on the split A2-site model originally proposed by Labbé.[20,32] The key feature of the model is split atomic positions for Pb in the pentagonal channels. This makes it possible to describe the ferroelectric structure with a $\sqrt{2} \times \sqrt{2} \times 1$ supercell relative to the aristotype $P4/mbm$, while the true cell is a four times larger $2\sqrt{2} \times \sqrt{2} \times 2$ cell with space group symmetry $Bb2_1m$.[20] The two models are related by the ordering of Pb inside the pentagonal channels, specifically an alternating in-plane displacement of Pb in the pentagonal channels in a direction normal to the polar axis. We assume here that the use of the simpler of these models does not significantly affect the discussion of the ferroelectric mechanism. Our HTXRD investigation of the ferroelastic strain (Figure 7b) supports this: the spontaneous strain associated with the ferroelectric transition consists of an expansion of the $b$ axis, referred to the $Cm2m$ setting used in Figure 1a, upon cooling through $T_C$. At the same time, the $a$ unit cell parameter demonstrates normal thermal contraction with no deviation from linearity. If the displacement pattern of Pb along $a$ plays a significant role in the


DOI: 10.1021/acs.chemmater.7b01817
Chem. Mater. XXXX, XXX, XXX−XXX

ferroelectric mechanism, one would expect the displacements to change abnormally upon approaching the Curie temperature, in turn affecting the *a* lattice parameter at $T_C$. No such behavior is observed, which we take as an indication that the split-site model captures the essential physics of the ferroelectric transition. We do note that the slope of the *c* unit cell parameter changes slightly close to $T_C$, but the effect is small compared to the change in *b*.

The lattice parameters and strain change continuously across $T_C$, as seen in Figures 7a and b, at least within the experimental uncertainty. This is in contrast to earlier works which report discontinuous changes in lattice parameters across $T_C$.[35,42] It is evident from Figure 7b that the strain does not follow the $(T_C - T)^{1/2}$ behavior expected from Landau theory for a continuous ferroelastic transition, which would require the slope to diverge at $T_C$. However, the strain is in this case a secondary order parameter, and its slope is not required to diverge at the transition unless it belongs to the same irrep as the primary order parameter.[43] *Cm*2*m* is an isotropy subgroup of *P*4/*mbm* belonging to the irrep $\Gamma_5^-$, which is the active irrep and primary order parameter for the transition.[30,40] The spontaneous strain, a shear strain in the *xy* plane referred to the *P*4/*mbm* aristotype, transforms as the irrep $\Gamma_4^+$, which is a secondary order parameter for the transition. In light of this, there is no reason to expect the spontaneous strain to behave as a good macroscopic order parameter for the phase transition.[36,44]

**Polarization and Ferroelectric Transition of PN.** The structure refinement, given the assumptions discussed above, leads to four particularly relevant cation configurations (Table 2). Interestingly, two of the configurations (1 and 2) have significantly lower energy than the two others, and these two are therefore in principle more likely to be the dominant configurations. At the same time, all configurations have a high spontaneous polarization, which is practically the same, approximately 109 $\mu$C cm$^{-2}$. This mirrors the behavior of the related system SBN, where a spontaneous polarization also exists for a large range of cation configurations.[25] As the calculated charge densities show (Figure 4), the polarization is due to a combination of Pb−O and Nb−O bonding cooperatively creating an in-plane polar distortion. The local coordination environment of Pb is reminiscent of that in tetragonal $PbTiO_3$,[8,45] where Pb tends to displace toward, and bond to, 4 of the 12 oxygen ions it is coordinated by on the A sites. The structure and charge densities in Figure 4 are consistent with the analysis performed by Labbé,[20] which concluded that both $Nb^{5+}$ and $Pb^{2+}$ contribute to the polarization through in-plane displacements. The same conclusion was also reached by Guo and colleagues in a similar analysis.[46] This particular behavior contrasts lead-free TTBs such as SBN and BNN ($Ba_{5-x}Na_{2x}Nb_{10}O_{30}$), where the A-site cations do not contribute significantly to the out-of-plane polarization, even though the space group symmetry allows for it.[20]

The spontaneous polarization calculated by DFT is 109 $\mu$C cm$^{-2}$, which is a very high value. As we are not aware of single crystal measurements of spontaneous polarization in pure PN, it is hard to directly compare this to experimental values. In fact, it was hypothesized early on that pure lead metaniobate has the character of a "frozen-in" ferroelectric,[42] in the sense that its spontaneous strain is too high to permit an easy reversal of the polarization at realistic electric field strengths. More data is available for the solid solution system $(Pb_xBa_{1-x})_5Nb_{10}O_{30}$ (PBN) than for pure PN, which is likely also due to the fact that solid solution stabilizes the TTB structure with respect to the nonferroelectric rhombohedral polymorph, making it easier to synthesize the material.[17] The PBN system is known to show significant improvements in piezoelectric properties over that of pure PN, with peak performance at around 40% Ba. Substitution of Ba for Pb in PBN presumably reduces the strain and makes it easier to switch the polarization.[42] For the composition $(Pb_{0.6}Ba_{0.4})_5Nb_{10}O_{30}$, a point charge calculation similar to the one performed here gave a polarization of 42 $\mu$C cm$^{-2}$, highly consistent with experimental values which lie in the range 38−46 $\mu$C cm$^{-2}$.[46] However, a calculation based on a simple point charge model captures only the ionic and not the electronic contribution to the polarization, whereas the Berry phase method includes both. In this sense, the value of 40 $\mu$C cm$^{-2}$ we obtain for pure PN should be regarded as a lower bound. This is also supported by the calculations of polarization in KBiN, where the point charge model gives a value of 33 $\mu$C cm$^{-2}$ and the Berry phase method 68 $\mu$C cm$^{-2}$, demonstrating that electronic contribution accounts for more than half of the total polarization.

The idea that pure PN has a high polarization which is not easily accessible in experiments is supported by the fact that ceramic samples generally show a low remanent polarization on the order of 1 $\mu$C cm$^{-2}$, while solid solutions of PN usually show an increased piezoelectric performance.[17] Finally, while the DFT values of spontaneous polarization obtained here are highly coherent, as shown in Figure 3b, they represent only four possible configurations in a structure which is inherently disordered. In our previous work, we considered the energetics of cation ordering in TTBs within the constraints of a 1 × 1 × 2 supercell, considering only the paraelectric state.[25] Within this framework, we found that there are several configurations with vacancies partially occupying A2 sites which are close in energy to the ones where vacancies are located on A1. Due to high vacancy diffusion barriers in TTBs, some degree of disorder is likely to freeze in during synthesis and persist down to ambient temperature. Such a cation disorder will reduce the polarization observed in the average *Cm*2*m* structure compared to the idealized cases we investigated here.

**Role of Lone Pairs in Ferroelectric TTBs.** The calculations for the KRN system suggest that the out-of-plane polar ($A_{2u}$) mode is an inherent feature of Nb-based TTB ferroelectrics. We have previously shown that a similar polar mode exists for a wide range of cation configurations in the unfilled SBN system[7] and hence can be described as robust with respect to cation−vacancy disorder. The results presented above therefore point to the strongly unstable in-plane polar ($E_u$) mode in KBiN as being the exception rather than the rule and closely linked to the presence of stereochemically active $Bi^{3+}$ on the A1 sites. In fact, calculations where $Tl^+$ (ionic radius 1.7 Å and stereochemically active) was substituted for $K^+$ (1.64 Å but no $6s^2$ lone pair) on the A2 sites, producing the compounds TlBiN and TlLaN, revealed that the additional presence of a lone pair cation on the A2 sites has only a negligible effect on the stability of the in-plane polarization.[47] The Tl compounds behave similarly to their K counterparts in that the out-of-plane polar instability is the most strongly unstable mode and that Bi on the A1 sites triggers an in-plane instability which is not present for any of the rare earth compounds.

What is the origin of the in-plane distortion for compounds with A1-site lone pair cations? In the undistorted aristotype TTB structure, the A1 site is similar to the 12-coordinated A


DOI: 10.1021/acs.chemmater.7b01817
Chem. Mater. XXXX, XXX, XXX−XXX

site in a cubic perovskite. The effect of the in-plane polar distortion seen in PN and in KBiN is to optimize the chemical bonding of Pb or Bi by making the coordination environment much less symmetric. One way to quantify this change based on crystallographic data is by the effective coordination number (ECoN). The calculation of ECoN is implemented in VESTA[48] and is defined as follows:[49]

$$\mathrm{ECoN} = \sum_i w_i,\ w_i = \exp\left[1 - \left(\frac{l_i}{l_{\mathrm{av}}}\right)^6\right] \quad (2)$$

$$l_{\mathrm{av}} = \frac{\sum_i l_i \exp[1 - (l_i/l_{\min})]}{\sum_i \exp[1 - (l_i/l_{\min})]} \quad (3)$$

The quantity $w_i$ in the above equations is a "bond weight" which describes the effective contribution of metal−oxygen bond $i$ to the coordination sphere of the metal cation, and $l_{\mathrm{av}}$ is to be interpreted as a weighted average bond length. For regular, undistorted polyhedra, the ECoN equals the nominal coordination number and decreases with increasing distortion. If the sum is taken over the 12 nominal bonds in the A1-site polyhedron of KBiN, we find that the ECoN for Bi changes from 11.9 in the high-symmetry structure to 5.4 when the in-plane polarization emerges. This is consistent with the asymmetric bonding visualized in Figure 10a. The ideal A1-site coordination number of 12 is never achieved in TTBs due to the octahedral connectivity requiring some degree of distortion even in the aristotype. The bonding environment for Pb or Bi in the distorted structures is reminiscent of that in tetragonal $PbTiO_3$, where Pb and O are arranged in a similar square-pyramidal coordination,[45] which is favored due to the well-known and strong Pb−O covalency.[8] The same Pb−O coordination is also found in $\alpha$-PbO (litharge)[50] and is due to Pb−O covalency similar to that in $PbTiO_3$.[51] This interaction and subsequent distortion therefore seems to be inherent to the lone pair cations $Pb^{2+}$ and $Bi^{3+}$. An important difference between the perovskite $PbTiO_3$ and the TTBs we focus on here, however, is the aforementioned slight distortion of the A1 site in the aristotype structure. The undistorted $BiO_{12}$ polyhedron in aristotype KBiN is slightly elongated in the out-of-plane $c$ direction with 4 short (2.60 Å) and 8 longer (2.69 Å) bonds. The shorter in-plane Bi−O bonds make it easier for an in-plane distortion to optimize chemical bonding than an out-of-plane distortion, and this is manifested in a much larger "lone pair effect" for the in-plane mode than the out-of-plane mode, directly demonstrated by comparison of Figures 9a and b. As a final observation, we note that the out-of-plane elongation of the A1-site polyhedra in TTBs is not reflected in the $c/a$ ratio as it would be in the perovskite structure. The HTXRD lattice parameters for PN (Figure 7a) show that the normalized $c/a < 1$ also in the high-symmetry structure, and the same holds for KBiN.

## CONCLUSION

The crystal structure of ferroelectric lead metaniobate was revised by a combination of X-ray and neutron powder diffraction. Refinements where Pb disorder was treated with a split-site model confirmed that lead preferentially occupies the pentagonal A2 sites in the TTB unit cell. DFT calculations based on the structural data gave a high spontaneous polarization of 109 $\mu$C cm$^{-2}$ for all relevant cation configurations, demonstrating that the ferroelectric polarization in PN is robust against cation−vacancy disorder. The calculations further confirmed that the in-plane polarization, which leads to orthorhombic symmetry, is stabilized by Pb−O covalency. The ferroelastic strain and the ferroelectric transition of PN at $T_C$ = (595 ± 5) °C was investigated by high temperature X-ray diffraction, which suggests that ordering of Pb on the A2 sites does not play a significant part in the phase transition mechanism. Calculations performed for the model system KRN provided evidence that an out-of-plane polarization is fundamental to Nb-based TTBs but that the presence of lone pair cations on the perovskite-like A1 sites can stabilize an in-plane polarization. In addition to PN, this effect is seen for $K_4Bi_2Nb_{10}O_{30}$ (KBiN), which has a spontaneous in-plane polarization of 68 $\mu$C cm$^{-2}$.

## AUTHOR INFORMATION


### Corresponding Author

*E-mail: tor.grande@ntnu.no.

### ORCID

Tor Grande: 0000-0002-2709-1219

### Present Address

§G.H.O.: School of Applied and Engineering Physics, Cornell University, Ithaca, New York 14853, United States.


### Author Contributions

G.H.O. performed the DFT calculations and did most of the experimental work with exception of neutron diffraction, which was performed by M.H.S. T.G. and S.M.S. supervised the project. G.H.O. wrote the paper with discussion and contributions from all authors.

### Notes

The authors declare no competing financial interest.

## ACKNOWLEDGMENTS

The Research Council of Norway (NFR Project 209337) and The Faculty of Natural Sciences at NTNU (ISP: "From molecules to process applications") are acknowledged for financial support. Computational resources were provided by Sigma2 (The Norwegian Metacenter for High Performance Computing) through Project NN9264K. G.H.O. thanks Ulrich Aschauer (University of Bern) for providing a convenient script for phonon calculations, and Elizabeth A. Nowadnick (Cornell) is thanked for enlightening discussions about symmetry and group theory.

## REFERENCES


(1) Lines, M. E.; Glass, A. M. *Principles and Applications of Ferroelectrics and Related Materials*; Oxford University Press: Oxford, 2001.

(2) Labbé, P. Tungsten Oxides, Tungsten Bronzes and Tungsten Bronze-Type Structures. *Key Eng. Mater.* **1992**, *68*, 293−0.

(3) Jamieson, P. B.; Abrahams, S. C.; Bernstein, J. L. Ferroelectric Tungsten Bronze-Type Crystal Structures. I. Barium Strontium Niobate $Ba_{0.27}Sr_{0.75}Nb_2O_{5.78}$. *J. Chem. Phys.* **1968**, *48*, 5048−5057.

(4) Abrahams, S. C.; Jamieson, P. B.; Bernstein, J. L. Ferroelectric Tungsten Bronze-Type Crystal Structures. III. Potassium Lithium Niobate $K_{6-x-y}Li_{4+x}Nb_{10+y}O_{30}$. *J. Chem. Phys.* **1971**, *54*, 2355−2364.

(5) Lundberg, M.; Sundberg, M. Studies of Phases in the $KNbO_3$−$Nb_2O_5$ System by High-Resolution Electron Microscopy and X-Ray Powder Diffraction. *J. Solid State Chem.* **1986**, *63*, 216−230.

(6) Goodman, G. Ferroelectric Properties of Lead Metaniobate. *J. Am. Ceram. Soc.* **1953**, *36*, 368−372.

(7) Olsen, G. H.; Aschauer, U.; Spaldin, N. A.; Selbach, S. M.; Grande, T. Origin of Ferroelectric Polarization in Tetragonal




DOI: 10.1021/acs.chemmater.7b01817
*Chem. Mater.* XXXX, XXX, XXX−XXX

Tungsten-Bronze-Type Oxides. *Phys. Rev. B: Condens. Matter Mater. Phys.* **2016**, *93*, 180101.
(8) Cohen, R. E. Origin of Ferroelectricity in Perovskite Oxides. *Nature* **1992**, *358*, 136−138.
(9) Seshadri, R.; Hill, N. A. Visualizing the Role of Bi 6s "Lone Pairs" in the Off-Center Distortion in Ferromagnetic $BiMnO_3$. *Chem. Mater.* **2001**, *13*, 2892−2899.
(10) Rödel, J.; Jo, W.; Seifert, K. T. P.; Anton, E.-M.; Granzow, T.; Damjanovic, D. Perspective on the Development of Lead-Free Piezoceramics. *J. Am. Ceram. Soc.* **2009**, *92*, 1153−1177.
(11) Lin, K.; Wu, H.; Wang, F.; Rong, Y.; Chen, J.; Deng, J.; Yu, R.; Fang, L.; Huang, Q.; Xing, X. Structure and Thermal Expansion of the Tungsten Bronze $Pb_2KNb_5O_{15}$. *Dalton Trans.* **2014**, *43*, 7037−7043.
(12) Schneck, J.; Toledano, J. C.; Whatmore, R.; Ainger, F. W. Incommensurate Phases in Ferroelectric Tetragonal Tungsten Bronzes. *Ferroelectrics* **1981**, *36*, 327−330.
(13) Levin, I.; Stennett, M. C.; Miles, G. C.; Woodward, D. I.; West, A. R.; Reaney, I. M. Coupling between Octahedral Tilting and Ferroelectric Order in Tetragonal Tungsten Bronze-Structured Dielectrics. *Appl. Phys. Lett.* **2006**, *89*, 122908.
(14) Zhu, X.; Fu, M.; Stennett, M. C.; Vilarinho, P. M.; Levin, I.; Randall, C. A.; Gardner, J.; Morrison, F. D.; Reaney, I. M. A Crystal-Chemical Framework for Relaxor versus Normal Ferroelectric Behavior in Tetragonal Tungsten Bronzes. *Chem. Mater.* **2015**, *27*, 3250−3261.
(15) Zhu, X. L.; Li, K.; Chen, X. M. Ferroelectric Transition and Low-Temperature Dielectric Relaxations in Filled Tungsten Bronzes. *J. Am. Ceram. Soc.* **2014**, *97*, 329−338.
(16) Randall, C. A.; Guo, R.; Bhalla, A. S.; Cross, L. E. Microstructure-Property Relations in Tungsten Bronze Lead Barium Niobate, $Pb_{1-x}Ba_xNb_2O_6$. *J. Mater. Res.* **1991**, *6*, 1720−1728.
(17) Sahini, M. G.; Grande, T.; Fraygola, B.; Biancoli, A.; Damjanovic, D.; Setter, N. Solid Solutions of Lead Metaniobate—Stabilization of the Ferroelectric Polymorph and the Effect on the Lattice Parameters, Dielectric, Ferroelectric, and Piezoelectric Properties. *J. Am. Ceram. Soc.* **2014**, *97*, 220−227.
(18) Hauback, B. C.; Fjellvåg, H.; Steinsvoll, O.; Johansson, K.; Buset, O. T.; Jørgensen, J. The High Resolution Powder Neutron Diffractometer PUS at the JEEP II Reactor at Kjeller in Norway. *J. Neutron Res.* **2000**, *8*, 215−232.
(19) Stinton, G. W.; Evans, J. S. O. Parametric Rietveld Refinement. *J. Appl. Crystallogr.* **2007**, *40*, 87−95.
(20) Labbé, P.; Frey, M.; Raveau, B.; Monier, J. C. Structure Cristalline de La Phase Ferroélectrique Du Niobate de Plomb $PbNb_2O_6$. Déplacements Des Atomes Métalliques et Interprétation de La Surstructure. *Acta Crystallogr., Sect. B: Struct. Crystallogr. Cryst. Chem.* **1977**, *33*, 2201−2212.
(21) Kresse, G.; Furthmüller, J. Efficient Iterative Schemes for Ab Initio Total-Energy Calculations Using a Plane-Wave Basis Set. *Phys. Rev. B: Condens. Matter Mater. Phys.* **1996**, *54*, 11169−11186.
(22) Perdew, J. P.; Ruzsinszky, A.; Csonka, G. I.; Vydrov, O. A.; Scuseria, G. E.; Constantin, L. A.; Zhou, X.; Burke, K. Restoring the Density-Gradient Expansion for Exchange in Solids and Surfaces. *Phys. Rev. Lett.* **2008**, *100*, 136406−136406.
(23) Kresse, G.; Joubert, D. From Ultrasoft Pseudopotentials to the Projector Augmented-Wave Method. *Phys. Rev. B: Condens. Matter Mater. Phys.* **1999**, *59*, 1758−1775.
(24) Monkhorst, H. J.; Pack, J. D. Special Points for Brillouin-Zone Integrations. *Phys. Rev. B* **1976**, *13*, 5188−5192.
(25) Olsen, G. H.; Selbach, S. M.; Grande, T. On the Energetics of Cation Ordering in Tungsten-Bronze-Type Oxides. *Phys. Chem. Chem. Phys.* **2015**, *17*, 30343−30351.
(26) Podlozhenov, S.; Graetsch, H. A.; Schneider, J.; Ulex, M.; Wöhlecke, M.; Betzler, K. Structure of strontium barium niobate $Sr_xBa_{1-x}Nb_2O_6$ (SBN) in the composition range $0.32 \leq x \leq 0.82$. *Acta Crystallogr., Sect. B: Struct. Sci.* **2006**, *62*, 960−965.
(27) Capillas, C.; Tasci, E. S.; de la Flor, G.; Orobengoa, D.; Perez-Mato, J. M.; Aroyo, M. I. A New Computer Tool at the Bilbao Crystallographic Server to Detect and Characterize Pseudosymmetry. *Z. Kristallogr.* **2011**, *226*, 186−196.
(28) Togo, A.; Tanaka, I. First Principles Phonon Calculations in Materials Science. *Scr. Mater.* **2015**, *108*, 1−5.
(29) Togo, A.; Tanaka, I. Evolution of Crystal Structures in Metallic Elements. *Phys. Rev. B: Condens. Matter Mater. Phys.* **2013**, *87*, 184104.
(30) Stokes, H. T.; Hatch, D. M.; Campbell, B. J. ISOTROPY Software Suite. iso.byu.edu.
(31) Chakraborty, K. R.; Sahu, K. R.; De, A.; De, U. Structural Characterization of Orthorhombic and Rhombohedral Lead Meta-Niobate Samples. *Integr. Ferroelectr.* **2010**, *120*, 102−113.
(32) Labbé, P.; Frey, M.; Allias, G. Nouvelles Données Structurales Sur La Variété Ferroélectrique Du Métaniobate de Plomb $PbNb_2O_6$. *Acta Crystallogr., Sect. B: Struct. Crystallogr. Cryst. Chem.* **1973**, *29*, 2204−2210.
(33) Shimakawa, Y.; Kubo, Y.; Nakagawa, Y.; Goto, S.; Kamiyama, T.; Asano, H.; Izumi, F. Crystal structure and ferroelectric properties of $ABi_2Ta_2O_9$ (*A* = Ca, Sr, and Ba). *Phys. Rev. B: Condens. Matter Mater. Phys.* **2000**, *61*, 6559−6564.
(34) Stokes, H. T.; Hatch, D. M. FINDSYM: Program for Identifying the Space-Group Symmetry of a Crystal. *J. Appl. Crystallogr.* **2005**, *38*, 237−238.
(35) Francombe, M. H.; Lewis, B. Structural, Dielectric and Optical Properties of Ferroelectric Lead Metaniobate. *Acta Crystallogr.* **1958**, *11*, 696−703.
(36) Salje, E. K. H. Crystallography and Structural Phase Transitions, an Introduction. *Acta Crystallogr., Sect. A: Found. Crystallogr.* **1991**, *47*, 453−469.
(37) Hewat, A. W. Cubic-Tetragonal-Orthorhombic-Rhombohedral Ferroelectric Transitions in Perovskite Potassium Niobate: Neutron Powder Profile Refinement of the Structures. *J. Phys. C: Solid State Phys.* **1973**, *6*, 2559.
(38) Megaw, H. D. Crystal Structure of Double Oxides of the Perovskite Type. *Proc. Phys. Soc.* **1946**, *58*, 133.
(39) Neurgaonkar, R. R.; Nelson, J. G.; Oliver, J. R.; Cross, L. E. Ferroelectric and structural properties of the tungsten bronze system $K_2Ln^{3+}Nb_5O_{15}$, Ln = La to Lu. *Mater. Res. Bull.* **1990**, *25*, 959−970.
(40) Orobengoa, D.; Capillas, C.; Aroyo, M. I.; Perez-Mato, J. M. AMPLIMODES: Symmetry-Mode Analysis on the Bilbao Crystallographic Server. *J. Appl. Crystallogr.* **2009**, *42*, 820−833.
(41) Olsen, G. H.; Sørby, M. H.; Hauback, B. C.; Selbach, S. M.; Grande, T. Revisiting the Crystal Structure of Rhombohedral Lead Metaniobate. *Inorg. Chem.* **2014**, *53*, 9715−9721.
(42) Francombe, M. H. The Relation between Structure and Ferroelectricity in Lead Barium and Barium Strontium Niobates. *Acta Crystallogr.* **1960**, *13*, 131−140.
(43) Stokes, H. T.; Hatch, D. M. Coupled Order Parameters in the Landau Theory of Phase Transitions in Solids. *Phase Transitions* **1991**, *34*, 53−67.
(44) Toledano, P. Phenomenological Approach to Structural Phase Transitions. *Key Eng. Mater.* **1992**, *68*, 1−42.
(45) Kuroiwa, Y.; Aoyagi, S.; Sawada, A.; Harada, J.; Nishibori, E.; Takata, M.; Sakata, M. Evidence for Pb-O Covalency in Tetragonal $PbTiO_3$. *Phys. Rev. Lett.* **2001**, *87*, 217601.
(46) Guo, R.; Evans, H. T., Jr.; Bhalla, A. S. Crystal Structure Analysis and Polarization Mechanisms of Ferroelectric Tetragonal Tungsten Bronze Lead Barium Niobate. *Ferroelectrics* **1998**, *206*, 123−132.
(47) Olsen, G. H. Ferroelectric Tungsten Bronzes. Ph.D. thesis, NTNU—Norwegian University of Science and Technology, Trondheim, Norway, 2016.
(48) Momma, K.; Izumi, F. VESTA 3 for Three-Dimensional Visualization of Crystal Volumetric and Morphology Data. *J. Appl. Crystallogr.* **2011**, *44*, 1272−1276.
(49) Hoppe, R.; Voigt, S.; Glaum, H.; Kissel, J.; Müller, H. P.; Bernet, K. A New Route to Charge Distributions in Ionic Solids. *J. Less-Common Met.* **1989**, *156*, 105−122.
(50) Leciejewicz, J. On the Crystal Structure of Tetragonal (Red) PbO. *Acta Crystallogr.* **1961**, *14*, 1304−1304.


DOI: 10.1021/acs.chemmater.7b01817
*Chem. Mater.* XXXX, XXX, XXX−XXX

(51) Watson, G. W.; Parker, S. C.; Kresse, G. Ab Initio Calculation of the Origin of the Distortion of α-PbO. *Phys. Rev. B: Condens. Matter Mater. Phys.* **1999**, *59*, 8481−8486.



DOI: 10.1021/acs.chemmater.7b01817
*Chem. Mater.* XXXX, XXX, XXX−XXX